PROGRESS REPORT

for the research performed under

NASA Research Grant NAG-1-643

by

Zafer Gürdal

John L. Phillips

Department of Engineering Science and Mechanics
Virginia Polytechnic Institute and State University
Blacksburg, VA 24061

Table of Contents

Abstract

This report summarizes the progress of the research supported by NASA Grant NAG-1-643. With the goal of tailorability in mind, the in-plane stiffness characteristics of a particular grid stiffened plate configuration under axial and shear loads have been studied. The contribution of the skin to the stiffener network and the resultant skin/rib interaction is analyzed. For the given plate geometry and loads, it is shown that an optimum configuration does exist.

In order to achieve optimally designed practical plate configurations, buckling constraints need to be included in the design. Due to the complex geometry and loading of the plates, a simplified local buckling analysis of isolated stiffeners and triangular skin elements between the stiffeners is considered. Development of a stiffener buckling analysis that represent stiffeners as shear deformable plate elements is presented.

Introduction

The potential advantages of applying grid stiffening concepts to composite structural components are numerous and varied. They include high stiffness-to-weight ratio, tailorability, damage tolerance, and economy of manufacture.

One of the earliest grid stiffening concepts was isogrid, so named for its pseudo-isotropic nature. While this may be appropriate for some applications, most structures have higher stiffness and strength requirements in specific directions. Thus it is expected that the efficiency of stiffened composite plates can be improved by tailoring their properties and geometries to meet the requirements of a specific application.

The work being performed for designing minimum weight grid stiffened plates under combined in-plane loadings is discussed in this report. The initial effort has concentrated on developing appropriate modelling of a basic element of this plate configuration in order to understand the response of these plates under the individual load cases. A parallel work concentrated on the development of a simplified buckling analysis of plate sub-components in order to incorporate practical stability constraints into the design procedure.

Stiffness Characterization

The work to date has focused on the in-plane stiffness characteristics of a grid stiffened composite plate under tension and shear loads. In general, a typical panel would consist of a laminated composite skin with a network of attached rectangular cross-section ribs, Figure 1. As shown in the figure, a single stiffened cell was isolated for analysis. The reasons for this are two-fold. First, in modelling a large panel with a repetitive stiffener pattern, geometric symmetry can be exploited to

reduce the problem to one of analyzing a single representative cell. Thus, a fine mesh can be used to model the component without incurring excessive computational expense. Secondly, some thought has been given to examining low width-to-length ratio structures, such as beams or ribs, where there may only be a single row of cells in one direction. With appropriate boundary conditions the same cell mesh can thus be used to model either a large panel or a slender member.

The particular cell under investigation was 254 mm (10 in) long by 147 mm (5.77 in) wide with a 60 degree included angle between the stiffeners in the axial direction. The skin thickness and stiffener width remained constant at 2.54 mm (0.1 in) and 19 mm (0.75 in) respectively. In line with current filament winding manufacturing techniques, the ribs were composed of unidirectional material. The skin was quasi-isotropic, with a (0/+45/-45/90) layup. Elastic properties were representative of a typical graphite-epoxy material.

Since the objective of this task was to study rib/skin interaction, a design variable 'stiffener ratio' (SR) was defined to be the ratio of stiffener height to skin thickness. The stiffener ratio of SR = 0 represents an unstiffened rectangular plate, while SR $\rightarrow \infty$ approaches a lattice grid (no attached skin). In practice, the lattice grid was modelled by setting the skin properties equal to zero.

Axial Loading Results

In this portion of the study, it was desired to model a representative portion of a large grid stiffened panel under uniform axial tensile load. As such, particular attention was paid to achieving the proper boundary conditions. To apply the axial load, a unit displacement in the x direction was imposed on all the nodes at one end while leaving them free in the y direction. However, it was found that the longitudinal edges had a tendency to curve or bow outward, see Figure 2. Caused by the ribs attempting to pivot or 'scissor' about the central node, the effect increased in severity

with larger stiffener ratios. While this behavior may be representative of a cell with free edges, for an internal section from a panel it violates displacement compatibility between neighboring cells. To eliminate the curvature, nodes along the longitudinal edges could simply be fixed in the transverse direction but left free in the axial direction. However, this restraint is probably not indicative of most applications (unless the panel were contained within a rigid frame) and results in artificially high axial stiffness values.

To model the longitudinal edges properly, it was desired to impose the condition that they remain straight, but still allow contraction/expansion in the transverse direction. This was achieved by adding a row of elements to each side of the plate, see Figure 3, with high transverse (E_2) and shear (G_{12}) moduli to reduce the edge curvature, but a very low axial (E_1) modulus so as to not alter the axial response of the panel. It was found that imposing the straight edge constraint with these beam like features increased the axial stiffness of all stiffened panels. The effect was more pronounced for higher stiffener ratios, rising to a maximum 5.4% improvement for SR = 10 (Figure 4).

As shown in Figure 4, the axial stiffness increased with thicker stiffeners, as expected. However, it is the structural efficiency on a weight basis, or equivalently the stiffness per unit volume (specific stiffness) which is of interest. Except for very low stiffener ratios, the efficiency of the panels decreases appreciably with increasing stiffener ratio, as indicated in Figure 5. At a stiffener ratio of SR = 10 the specific stiffness is only 50% of that for an unstiffened panel. Consistent with this trend, the specific stiffness for a lattice grid was extremely low at 0.0364 N/mm^4, which represents just 4.4% of the unstiffened plate value.

The panels appear to be relatively flexible under axial loading because of the stiffeners' tendency to scissor together. Therefore, as the stiffener ratio becomes larger, the skin is less effective in controlling this action. Transverse contraction of

the panel became increasingly pronounced with the higher stiffener ratios, and in particular the lattice panel (Figure 6).

At very small stiffener ratios the specific stiffness increased with increasing stiffener ratio and reached a peak, indicating an optimum value of the stiffener ratio. It is believed that the small increase in specific stiffness at the low stiffener ratio was due more in part to laminate ply synergism than to geometric stiffening effects. Figure 7 shows that the addition of a small amount of 30 degree material to the quasi-isotropic substrate results in an increased E_x for the stiffener material. Therefore, the material itself became stiffer, resulting in improved panel stiffness. Unfortunately, this effect only appeared at very low stiffener ratios, with the trend to lower moduli giving reduced specific stiffness for the panels above SR = 0.25.

From these results, it would appear that this grid configuration is not well suited to axial loading. Since the primary mode of deformation appeared to involve rotation of the stiffeners, some means of controlling this would likely show substantial efficiency improvements. This might take the form of transverse stiffeners at the nodes, which results in isogrid, or employing an anisotropic skin with increased transverse stiffness.

Shear Loading Results

The problems associated with modelling a panel under shear loads were similar to those encountered for the axial case. That is, it was desired to constrain all edges to remain straight but still allow free contraction or expansion in both the axial and transverse directions. This was eventually accomplished by adding a second pair of rows of elements to the ends of the panel. The shear loading was applied by imposing a unit displacement in the direction of the diagonal, with the opposing node fixed (Figure 8).

Qualitatively, the results were somewhat similar to those for axial loading. With increasing stiffener ratio, the shear stiffness rose concurrently (Figure 9). However, the peak shear stiffness for SR = 10 was 160% higher than that for SR = 0, whereas the equivalent increase for the axial case was only 90%. On a weight (volume) basis, the specific shear stiffness again decreased significantly after an early peak (Figure 10). Although the improvement at low stiffener ratio was considerably more pronounced than for the axial case, the increase was still limited to only about 4% over the unstiffened plate, at a SR = 0.4. For higher stiffener ratios, the degradation in specific shear stiffness was not as severe as that for the axial case. For example, at a stiffener ratio of SR = 10 the shear panel retained 69% of the unstiffened plate stiffness, versus only 50% for the axial case. The lattice panel had a specific shear stiffness equal to 0.155 N/mm^4, which represents 44% of the plate value. This displays a considerable improvement over the lattice grid under axial loads, which only retained 4.4% of the corresponding unstiffened plate stiffness. Also, the deformed lattice grid does not appear significantly different than the stiffened panels (Figure 11), which again differs from the behavior under axial loading (Figure 6).

In summary, the stiffened panel behaved similarly to the axial panel in a qualitative sense. Quantitatively, the shear panel appeared to be more sensitive to the changes at low stiffener ratios, but less prone to degradation in specific stiffness with increasing stiffener ratio. The lattice grid in particular displayed much improved performance over its axial counterpart.

Summary of Stiffness Characterization

Imposing suitable boundary conditions on the stiffened cells (i.e. the straight edge constraint) was found to have a significant effect on the results obtained. In the shear case, the addition of beams was essential to distribute the nodal point loads, eliminating gross local deformations. These results highlight the need to model specimen boundary conditions as accurately as possible.

For both the axial and shear loaded plates, an optimum specific stiffness existed at very low stiffener ratios. Although this effect was more pronounced for the shear case, the increase was still relatively small. Aside from this modest initial increase, the general trend was to decreasing specific stiffness for increasing stiffener ratio. The limiting case was provided by the lattice grids, which displayed poor specific stiffness, especially so for the axially loaded example. This result suggested that in order to increase the efficiency of the grid stiffened panel under axial and shear loads, it is essential to control the scissoring of the stiffeners.

For the rib plus attached skin panel, preventing the scissoring action might include using an anisotropic skin with increased stiffness in the transverse direction. In addition, the results for very low stiffener ratios hinted that it may be possible to improve the stiffener material properties via judicious choices of rib and skin ply combinations. For either the skinned or the lattice panel, the addition of transverse stiffeners at the nodes should also result in substantial improvement in panel stiffness due to triangulation of the structure. Of course, adding transverse members of the same thickness as the original ribs would result in isogrid, with its attendant pseudo-isotropic behavior. However, if the panel were to support loads of a directional nature, it would likely be possible to adjust the thickness or width of the ribs individually to arrive at a reduced weight configuration.

Stability Constraints

The in-plane stiffness analyses of the previous section were conducted without any type of buckling constraints imposed on the designs. Thus, for maximum specific stiffness, a design was similar to that of a flat plate with rather low stiffeners. However, intuitively one expects that in practice the performance of this structure would be poor due to its low out-of-plane bending stiffness, and thus attendant low resistance to buckling under compressive loads. Besides the constraints on specific stiffness and local failures associated with the material strength failure in the stiffeners and the skin panels, constraints against stability failures must be included in the design in order to achieve meaningful structures. Global buckling of the panel, as well as the local buckling of the skin between the stiffeners and the stiffeners themselves must be included in the optimization process.

In evaluating the suitability of various proposed buckling schemes, it should be noted that verification of the model appears to be difficult. Experimental results in the literature for buckling tests on grid stiffened composite panels are very limited. The data that is reported often exhibits a considerable amount of scatter, generally thought to be a result of manufacturing imperfections. Due to the complex geometry of the panels, an exact analytical solution does not exist. The best estimate of panel response may be that provided by a detailed finite element (FE) analysis, which may result in a prohibitively expensive design optimization run. Rather than performing a sophisticated finite elements buckling analysis of the grid stiffened plate, the approach used in the present study is to use simplified buckling analysis of the overall plate and the individual components. Following is the development of the procedure for the buckling analysis of the stiffeners.

Stiffener Buckling Failure

Grid stiffened fiber-reinforced composite plates are primarily manufactured as filament-wound structures. The filament winding process as an economical method of fabrication makes the grid stiffened structural concept attractive. For stiffeners with unidirectional fibers, the stiffener material is orthotropic with respect to the stiffener axis. For typical high performance composite materials, the shear stiffness of such a configuration will be low compared with the longitudinal modulus of the material. Even for stiffeners which are laminated with plies of various angular orientations, the transverse shear stiffness is low. The low transverse shear stiffness, combined with the possibility of low ratios of stiffener length to thickness ratio, point to the importance of the effects of transverse shear deformations in computing the buckling load for a stiffener. With this point in mind, a procedure is developed to predict the critical end load for a composite stiffener. The stiffener is assumed to be a simple blade type, and thus is treated as a rectangular plate with one edge joining the skin, the opposite edge away from the skin free, and the other two edges loaded uniformly along the stiffener axis. The loads for the stiffeners are calculated from the finite analysis of the plate already performed for the stresses and displacements. The boundary conditions at the loaded edges of the stiffeners are probably between that of simply supported and fixed conditions, with indications in the literature that it is closer to a fixed condition. In considering anticipated buckling modes, if the stiffeners are assumed to buckle simultaneously with the triangular skin sub-elements, then the hub of the stiffeners would undergo no rigid-body rotation, so that the stiffener end would be fixed except for a small amount of flexibility in the hub. One possible treatment is to assume that the stiffener ends are fixed, but that the effective stiffener length is greater than the exposed stiffener length by some fraction of the hub diameter. Because many of the earlier works have considered simply supported ends than fixed ends, the computational procedure developed here for the simply supported end conditions. This will result in an conservative design results.

In the following analysis the stiffener plate is considered to be a laminated composite material which is orthotropic with respect to the stiffener axis. First order shear deformation theory is used in a Rayleigh-Ritz procedure to solve for the critical buckling load and the buckling mode shape.

Buckling Calculations

Theory

The stiffener is treated as a rectangular plate supported on three edges, with a uniform compressive load, N', applied at the two opposing supported edges. The plate dimensions and coordinate axes are shown in Figure 12. The plate material is assumed to an orthotropic composite laminate. The plate theory used is the first-order transverse shear deformation theory for plates, in which shear deformation is assumed to be linear through the thicknesses.

The assumed displacement field in the plate is given by

$$\begin{aligned} u_1(x,y,z) &= u(x,y) + Z\phi_x(x,y) \\ u_2(x,y,z) &= v(x,y) + Z\phi_y(x,y) \\ u_3(x,y,z) &= w(x,y) \end{aligned} \tag{1}$$

where u_1, u_2, and u_3 are the displacement components in the x, y, and z directions, respectively, u, v, and w are the corresponding displacements of the mid-plane of the plate, and ϕ_x and ϕ_y are the rotations due to bending of a material line initially perpendicular to the mid-plane, about the y- and x-axes, respectively. (Using the right hand rule, the sense of the rotations are $\hat{j}$ for ϕ_x , and $-i$ for ϕ_y.) The strain-displacement relation for small displacements,

$$E_{ij} = \frac{1}{2}(u_{i,j} + u_{j,i}) \tag{2}$$

results in the following expressions for strains:

$$
\begin{aligned}
E_1 &= E_{11} = \frac{\partial u}{\partial x} + z\frac{\partial \phi_x}{\partial x} \\
E_2 &= E_{22} = \frac{\partial v}{\partial y} + z\frac{\partial \phi_y}{\partial y} \\
E_6 &= E_{12} = \frac{1}{2}\left[\frac{\partial u}{\partial y} + \frac{\partial v}{\partial x} + z\left(\frac{\partial \phi_x}{\partial y} + \frac{\partial \phi y}{\partial x}\right)\right] \\
E_4 &= E_{23} = \frac{1}{2}\left(\phi_y + \frac{\partial w}{\partial y}\right) \\
E_5 &= E_{13} = \frac{1}{2}\left(\phi_x + \frac{\partial w}{\partial x}\right) \\
E_3 &= E_{33} = 0
\end{aligned}
\tag{3}
$$

Energy considerations can be used to derive the differential equations of equilibrium for the plate. Assuming a linearly elastic material, the strain energy of the plate, U, can be written as

$$U = \int_{\Omega} \int_{\frac{-h}{2}}^{\frac{h}{2}} \frac{1}{2}\sigma_{ij}\varepsilon_{ij} dz d\Omega \tag{4}$$

where Ω is the domain of the plate in the x-y plane. The potential energy of the applied loads, V, is

$$V = -\int_{S_2} \hat{t}_i u_i dS_2 \tag{5}$$

where S_2 is the portion of the plate surface where a traction t is applied. The total potential energy, Π, is

$$\Pi = U + V \tag{6}$$

and by the principle of minimum total potential energy, the variation of the total potential energy is zero, or

$$\delta\Pi = 0 \tag{7}$$

When the loading applied to the plate is limited to in-plane edge loads, the resulting system of equations corresponding to virtual displacements of the five displacement variables, u, v, w, ϕ_x, and ϕ_y, are:

$$\begin{aligned}
&\frac{\partial N_1}{\partial x} + \frac{\partial N_6}{\partial y} = 0 \\
&\frac{\partial N_6}{\partial x} + \frac{\partial N_2}{\partial y} = 0 \\
&\frac{\partial Q_1}{\partial x} + \frac{\partial Q_2}{\partial y} + N = 0 \\
&\frac{-\partial M_1}{\partial x} - \frac{\partial M_6}{\partial y} + Q_1 = 0 \\
&\frac{-\partial M_6}{\partial x} - \frac{\partial M_2}{\partial y} + Q_2 = 0
\end{aligned} \tag{8}$$

where the in-plane edge force resultants, N_i, the moment resultants, M_i, and the edge shear force resultants, Q_i , are given by

$$\begin{aligned}
\begin{bmatrix} N_i \\ M_i \end{bmatrix} &= \int_{\frac{-h}{2}}^{\frac{h}{2}} \begin{bmatrix} 1 \\ z \end{bmatrix} \sigma_i dz \qquad i = 1, 2, 6 \\
\begin{bmatrix} Q_1 \\ Q_2 \end{bmatrix} &= \int_{\frac{-h}{2}}^{\frac{h}{2}} \begin{bmatrix} \sigma_5 \\ \sigma_4 \end{bmatrix} dz
\end{aligned} \tag{9}$$

and the transverse force term, N, is

$$N = N_1 \frac{\partial^2 w}{\partial x^2} + N_2 \frac{\partial^2 w}{\partial y^2} + Z N_6 \frac{\partial^2 w}{\partial x \partial y} \tag{10}$$

which arises by considering the projection of the in-plane force resultants on the z-axis for the case where the plate is deflected.

To treat the buckling of a plate stiffener, consider the following boundary load conditions:

$$\begin{aligned} x = 0, \ell: \quad & N_1 = -N'_x \quad N_6 = 0 \\ y = 0, b: \quad & N_2 = 0 \quad N_6 = 0 \end{aligned} \tag{11}$$

From the first two of equations (8), we have the solution that

$$\begin{aligned} & N_1(x,y) = -N'_x = \text{Const} \\ & N_2(x,y) = 0 \qquad\qquad \text{in } \Omega \\ & N_6(x,y) = 0 \end{aligned} \tag{12}$$

so that we can now limit our consideration to the following three equilibrium equations:

$$\begin{aligned} & \frac{\partial Q_1}{\partial x} + \frac{\partial Q_2}{\partial y} = N'_x \frac{\partial^2 w}{\partial x^2} \\ & \frac{-\partial M_1}{\partial x} - \frac{\partial M_6}{\partial y} + Q_1 = 0 \\ & \frac{-\partial M_6}{\partial x} - \frac{\partial M_2}{\partial y} + Q_2 = 0 \end{aligned} \tag{13}$$

Consider the constitute equations for an orthotropic lamina with respect to its principle axes. For the transverse shear, we have the relations

$$\begin{aligned} \sigma_4 = \sigma_{23} = 2C_{44}\varepsilon_4 = 2G_{23}\varepsilon_4 \\ \sigma_5 = \sigma_{13} = 2C_{55}\varepsilon_5 = 2G_{13}\varepsilon_5 \end{aligned} \tag{14}$$

where the symbols will be defined presently. The constitutive equations relating the in-plane stresses and strains are those for an orthotropic plate where the transverse normal stress is zero, and in summary we have the following constitutive relations:

$$\begin{Bmatrix} \sigma_1 \\ \sigma_2 \\ \sigma_4 \\ \sigma_5 \\ \sigma_6 \end{Bmatrix} = \begin{bmatrix} Q_{11} & Q_{12} & 0 & 0 & 0 \\ Q_{12} & Q_{22} & 0 & 0 & 0 \\ 0 & 0 & 2C_{44} & 0 & 0 \\ 0 & 0 & 0 & 2C_{55} & 0 \\ 0 & 0 & 0 & 0 & 2Q_{66} \end{bmatrix} \begin{Bmatrix} \varepsilon_1 \\ \varepsilon_2 \\ \varepsilon_4 \\ \varepsilon_5 \\ \varepsilon_6 \end{Bmatrix} \tag{15}$$

where the same contracted notation is used for stresses, σ_i as was introduced for strains in equations (3), and where

$$Q_{11} = \frac{E_1}{1 - \gamma_{12}\gamma_{2i}} \qquad Q_{22} = \frac{E_2}{1 - \gamma_{12}\gamma_{21}} \qquad Q_{12} = \frac{\gamma_{12}E_2}{1 - \gamma_{12}\gamma_{21}} \tag{16}$$
$$C_{44} = G_{23} \qquad C_{55} = G_{13} \qquad Q_{66} = G_{12}$$

where E_1 and E_1 are Young's moduli, γ_{12} and γ_{21} are Poisson's ratios, and G_{23}, G_{13} and G_{12} are shear moduli, the subscripts having the usual meanings.

To transform the constitutive relations for the lamina to an arbitrary coordinate transformation,

$$\begin{Bmatrix} x \\ y \\ z \end{Bmatrix} = \begin{bmatrix} \cos\theta & -\sin\theta & 0 \\ \sin\theta & \cos\theta & 0 \\ 0 & 0 & 1 \end{bmatrix} \begin{Bmatrix} x' \\ y' \\ z' \end{Bmatrix} \tag{17}$$

or

$$\{X_i\} = [t_{ij}] \{X'_j\} \tag{18}$$

where the primed axes are the principle orthotropic axes. The the transformation for a fourth order tensor is

$$\overline{T}_{ijkl} = t_{im}t_{jn}t_{kr}t_{ls}T_{mnrs} \tag{19}$$

where $\overline{T}_{ijkl}$ is in the unprimed axis system. Noting that in expanded notation

$$Q_{16} = A_{1112}, \qquad C_{44} = C_{2323}, \qquad \text{etc.} \tag{20}$$

the transformation results in

$$\begin{aligned}
\overline{Q}_{11} &= Q_{11}\cos^4\theta + z(Q_{12} + 2Q_{66})\sin^2\theta\cos^2\theta + Q_{22}\sin^4\theta \\
\overline{Q}_{12} &= (Q_{11} + Q_{22} - 4Q_{66})\sin^2\theta\cos^2\theta + Q_{12}(\sin^4\theta + \cos^4\theta) \\
\overline{Q}_{22} &= Q_{11}\sin^4\theta + z(Q_{12} + 2Q_{66})\sin^2\theta\cos^2\theta + Q_{22}\cos^4\theta \\
\overline{Q}_{16} &= (Q_{11} - Q_{12} - 2Q_{66})\sin\theta\cos^3\theta + (Q_{12} - Q_{22} + 2Q_{66})\sin^3\theta\cos\theta \\
\overline{Q}_{26} &= (Q_{11} - Q_{12} - 2Q_{66})\sin^3\theta\cos\theta + (Q_{12} - Q_{22} + 2Q_{66})\sin\theta\cos^3\theta \\
\overline{Q}_{66} &= (Q_{11} + Q_{22} - 2Q_{12} - 2Q_{66})\sin^2\theta\cos^2\theta + Q_{66}(\sin^4\theta + \cos^4\theta) \\
\overline{C}_{44} &= C_{44}\cos^2\theta + C_{55}\sin^2\theta \\
\overline{C}_{55} &= C_{55}\cos^2\theta + C_{44}\sin^2\theta \\
\overline{C}_{45} &= (C_{44} - C_{55})\cos\theta\sin\theta
\end{aligned} \tag{21}$$

Substituting in the expression for strains in terms of the assumed displacements, the constitutive relations in the unprimed axis system are

$$\begin{Bmatrix} \sigma_1 \\ \sigma_2 \\ \sigma_6 \\ \sigma_4 \\ \sigma_5 \end{Bmatrix} = \begin{bmatrix} \overline{Q}_{11} & \overline{Q}_{12} & \overline{2Q}_{16} & 0 & 0 \\ \overline{Q}_{21} & \overline{Q}_{22} & \overline{2Q}_{26} & 0 & 0 \\ \overline{Q}_{16} & \overline{Q}_{26} & \overline{2Q}_{66} & 0 & 0 \\ 0 & 0 & 0 & \overline{2C}_{44} & \overline{2C}_{45} \\ 0 & 0 & 0 & \overline{2C}_{45} & \overline{2C}_{55} \end{bmatrix} \begin{Bmatrix} u_{,x} + z\phi_{x,x} \\ v_{,y} + z\phi_{y,y} \\ \frac{1}{2}\left[u_{,y} + v_{,x} + z(\phi_{x,y} + \phi_{y,x})\right] \\ \frac{1}{2}\left(\phi_y + \frac{\partial w}{\partial y}\right) \\ \frac{1}{2}\left(\phi_x + \frac{\partial w}{\partial x}\right) \end{Bmatrix} \tag{22}$$

Consider a laminate made of k orthotropic layers, each oriented at some angle with respect to the reference axes. Integrate equation (22) over the thickness to get the following constitutive relations between the resultants of equations (9) and the assumed displacements:

$$\begin{Bmatrix} N_1 \\ N_2 \\ N_6 \\ M_1 \\ M_2 \\ M_6 \end{Bmatrix} = \begin{bmatrix} A_{11} & A_{12} & A_{16} & B_{11} & B_{12} & B_{16} \\ . & A_{22} & A_{26} & B_{12} & B_{22} & B_{26} \\ . & . & A_{66} & B_{16} & B_{26} & B_{66} \\ . & . & . & D_{11} & D_{12} & D_{16} \\ . & SYM & . & . & D_{22} & D_{26} \\ . & . & . & . & . & D_{66} \end{bmatrix} \begin{Bmatrix} u_{,x} \\ v_{,y} \\ u_{,y} + v_{,x} \\ \phi_{x,x} \\ \phi_{y,y} \\ \phi_{x,y} + \phi_{y,x} \end{Bmatrix} \qquad (23)$$

$$\begin{Bmatrix} Q_2 \\ A_1 \end{Bmatrix} = K^2 \begin{bmatrix} A_{44} & A_{45} \\ A_{45} & A_{45} \end{bmatrix} \begin{Bmatrix} \phi_y + w_{,y} \\ \phi_x + w_{,x} \end{Bmatrix}$$

where K^2 is the commonly used shear correction factor, assumed here to be (5/6), and

$$\begin{bmatrix} A_{ij} \\ B_{ij} \\ D_{ij} \end{bmatrix} = \sum_{k=1}^{N} \int_{h_{k-1}}^{h_k} \overline{Q}_{ij}^k \begin{bmatrix} 1 \\ z \\ z^2 \end{bmatrix} dz = \sum_{k=1}^{N} \overline{Q}_{ij}^k \begin{bmatrix} (h_k - h_{k-1}) \\ \frac{1}{2}(h_k^2 - h_{k-1}^2) \\ \frac{1}{3}(h_k^2 - h_{k-1}^3) \end{bmatrix} \quad i,j = 1,\ 2,\ 6 \qquad (24)$$

$$A_{ij} = \sum_{k=1}^{N} \int_{h_{k-1}}^{h_k} \overline{C}_{ij}^k dz = \sum_{k=1}^{N} \overline{C}_{ij}^k (h_k - h_{k-1}) \qquad i,\ j = 4,\ 5$$

where h_{k-1} and h_k are the z-coordinates of the lower and upper surfaces, respectively (positive z being up), of the k-th lamina with respect to the mid-plane of the plate.

We now restrict consideration to laminates which are orthotropic with respect to the reference axes. These include unidirectional and symmetric cross-ply laminates. For these laminates, $B_{ij} = 0$, $i,j = 1,2,6$, and $A_{16} = A_{26} = D_{16} = D_{26} = 0$. For an orthotropic material, equations (23) reduce to

$$
\begin{aligned}
N_1 &= A_{11}\frac{\partial u}{\partial x} + A_{12}\frac{\partial v}{\partial y} & N_6 &= A_{66}\left(\frac{\partial u}{\partial y} + \frac{\partial v}{\partial x}\right) \\
N_2 &= A_{12}\frac{\partial u}{\partial x} + A_{22}\frac{\partial v}{\partial y} & & \\
M_1 &= D_{11}\frac{\partial \phi_x}{\partial x} + D_{12}\frac{\partial \phi_y}{\partial y} & M_6 &= D_{66}\left(\frac{\partial \phi_x}{\partial y} + \frac{\partial \phi_y}{\partial x}\right) \\
M_2 &= D_{12}\frac{\partial \phi_x}{\partial x} + D_{22}\frac{\partial \phi_y}{\partial y} & & \\
Q_1 &= K^2 A_{55}\left(\phi_x + \frac{\partial w}{\partial x}\right) & & \\
Q_2 &= K^2 A_{44}\left(\phi_y + \frac{\partial w}{\partial y}\right) & &
\end{aligned}
\tag{25}
$$

To employ the Rayleigh-Ritz procedure, begin by recreating the variational statements used in deriving the governing differential equations. Multiply the three equations (13) by the virtual displacements δw, $\delta \phi_x$, and $\delta \phi_y$, respectively, and integrate over the x-y domain of the plate:

$$
\begin{aligned}
&\int_\Omega \left(\frac{\partial Q_1}{\partial x} + \frac{\partial Q_2}{\partial y} - N'_x \frac{\partial^2 w}{\partial x^2}\right)\delta w d\Omega = 0 \\
&\int_\Omega \left(\frac{-\partial M_1}{\partial x} - \frac{\partial M_6}{\partial y} + Q_1\right)\delta \phi_x d\Omega = 0 \\
&\int_\Omega \left(\frac{-\partial M_6}{\partial x} - \frac{\partial M_2}{\partial y} + Q_2\right)\delta \phi_y d\Omega = 0
\end{aligned}
\tag{26}
$$

Integrate by parts and apply Gauss' divergence theorem to get

$$\int_{\Omega}\left(\frac{\partial\delta w}{\partial x}Q_1+\frac{\partial\delta w}{\partial y}Q_2-\frac{\partial\delta w}{\partial x}N'_x\frac{\partial w}{\partial x}\right)dxdy=\int_S S_z\delta w ds$$
$$\int_{\Omega}\left(\frac{\partial\delta\phi_x}{\partial x}M_1+\frac{\partial\delta\phi_x}{\partial y}M_6+\delta\phi_x Q_1\right)dxdy=\int_S M_x\delta\phi_x ds \qquad (27)$$
$$\int_{\Omega}\left(\frac{\partial\delta\phi_y}{\partial x}M_6+\frac{\partial\delta\phi_y}{\partial y}M_2+\delta\phi_y Q_2\right)dxdy=\int_S M_y\delta\phi_y ds$$

where

$$S_x=\left(Q_1-N'_x\frac{\partial w}{\partial x}\right)n_x+Q_2n_y$$
$$M_x=M_1n_x+M_6n_y \qquad (28)$$
$$M_y=M_6n_x+M_2n_y$$

where n_x and n_y are the in-plane components of the unit normal vector at the boundary of the plate.

For plates with a combination of simply supported (S.S), fixed, and free edges, the RHS terms of equations (27) are identically zero, since on all boundaries either the respective displacement components are specified and have a zero variation, or the resultant generalized force components are zero. We introduce approximate solutions for w, ϕ_x, and ϕ_y in the following form:

$$w\doteq\sum_{i=1}^{N_w}A_i\psi_i(x,y) \qquad \phi_x\doteq\sum_{i=1}^{N_{\phi_x}}B_i\theta_{xi}(x,y) \qquad \phi_{yy}\doteq\sum_{i=1}^{N_{\phi_y}}C_i\theta_{yi}(x,y) \qquad (29)$$

where $\psi_i(x,y)$, $\theta_{xi}(x,y)$, and $\theta_{yi}(x,y)$ are shape functions which satisfy the geometric boundary conditions and which are part of a complete set, and A_i, B_i, and C_i are constant coefficients to be determined. The variations which appear in equations (27) now become

$$\delta w = \sum_{i=1}^{N_w} \delta A_i \psi_i(x,y)$$

$$\delta \phi_x = \sum_{i=1}^{N_{\phi_x}} \delta B_i \theta_{xi}(x,y) \qquad \delta \phi_y = \sum_{i=1}^{N_{\phi_y}} \delta C_i \theta_{yi}(x,y) \tag{30}$$

When equations (29) and (30) are substituted into equations (27) and the variation of each coefficient seen in equations (30) is taken to be independent of the others, the following system of equations results:

$$\sum_{j=1}^{N_w} K_{ij}^{11} A_j + \sum_{j=1}^{N_{\phi_x}} K_{ij}^{12} B_j + \sum_{j=1}^{N_{\phi_y}} K_{ij}^{13} C_j = N'_x \sum_{j=1}^{N_w} M_{ij} A_j \quad i = 1,2,...,N_w$$

$$\sum_{j=1}^{N_w} K_{ij}^{21} A_j + \sum_{j=1}^{N_{\phi_x}} K_{ij}^{22} B_j + \sum_{j=1}^{N_{\phi_y}} K_{ij}^{23} C_j = 0 \quad i = 1,2,..., N_{\phi_x} \tag{31}$$

$$\sum_{j=1}^{N_w} K_{ij}^{31} A_j + \sum_{j=1}^{N_{\phi_x}} K_{ij}^{32} B_j + \sum_{j=1}^{N_{\phi_y}} K_{ij}^{33} C_j = 0 \quad i = 1,2,..., N_{\phi_y}$$

where

$$
\begin{aligned}
M_{ij} &= \int_0^{\ell}\int_0^{b} \frac{\partial \psi_i}{\partial x}\frac{\partial \psi_j}{\partial x}dydx \\
K_{ij}^{11} &= \int_0^{\ell}\int_0^{b} K^2\left(A_{55}\frac{\partial \psi_i}{\partial x}\frac{\partial \psi_j}{\partial x} + A_{44}\frac{\partial \psi_i}{\partial y}\frac{\partial \psi_j}{\partial y}\right)dydx \\
K_{ij}^{12} = K_{ji}^{21} &= \int_0^{\ell}\int_0^{b} K^2\left(A_{55}\frac{\partial \psi_i}{\partial x}\theta_{xj}\right)dydx \\
K_{ij}^{13} = K_{ji}^{31} &= \int_0^{\ell}\int_0^{b} K^2\left(A_{44}\frac{\partial \psi_i}{\partial y}\theta_{yj}\right)dydx \\
K_{ij}^{22} &= \int_0^{\ell}\int_0^{b} \left(D_{11}\frac{\partial \theta_{xi}}{\partial x}\frac{\partial \theta_{xj}}{\partial x} + D_{66}\frac{\partial \theta_{xj}}{\partial y}\frac{\partial \theta_{xj}}{\partial y} + K^2 A_{55}\theta_{xi}\theta_{xj}\right)dydx \\
K_{ij}^{23} = K_{ji}^{32} &= \int_0^{\ell}\int_0^{b} \left(D_{12}\frac{\partial \theta_{xi}}{\partial x}\frac{\partial \theta_{yj}}{\partial y} + D_{66}\frac{\partial \theta_{xi}}{\partial y}\frac{\partial \theta_{yj}}{\partial x}\right)dydx \\
K_{ij}^{33} &= \int_0^{\ell}\int_0^{b} \left(D_{22}\frac{\partial \theta_{yi}}{\partial y}\frac{\partial \theta_{yj}}{\partial y} + D_{66}\frac{\partial \theta_{yi}}{\partial x}\frac{\partial \theta_{yj}}{\partial x} + K^2 A_{44}\theta_{yi}\theta_{yj}\right)dydx
\end{aligned}
\tag{32}
$$

Equations (31) can be reduced to a symbolic form as follows which has the form of an eigenvalue problem.

$$
\left[[\bar{A}^{11}] - N'_x[\bar{M}]\right]\{A\} = \{0\} \tag{33}
$$

For the critical buckling condition the determinant of the matrix in equation (33) must be zero, and the resulting eigenvalues, N'_x, are the approximate critical buckling loads corresponding to various approximate buckling mode shapes. The lowest critical value of N'_x identified, is the approximate buckling load of interest.

The required two-dimensional shape functions are chosen here to be built as products of pairs of one-dimensional shape functions, one being a function of x, the other, a function of y. The following notation for indexing and dimensioning is used:

$$w = \psi_i(x,y) = f_m^{(1)}(x) g_n^{(1)}(y), \quad m = 1,2,...,N_{wx}, \quad n = 1,2,...N_{wy},$$
$$i = (m-1)N_{wy} + n, \quad N_w = N_{wx} N_{wy}$$

$$\phi_x = \phi_{\xi}(x,y) = f_m^{(2)}(x) g_n^{(2)}(y), \quad m = 1,2,...,N_{\phi xx}, \quad n = 1,2,...N_{\phi xy}, \tag{34}$$
$$i = (m-1)N_{\phi xy} + n, \quad N_{\phi x} = N_{\phi xx} N_{\phi xy}$$

$$\phi_y = \phi_{yi}(x,y) = f_m^{(3)}(x) g_n^{(3)}(y), \quad m = 1,2,...,N_{\phi yx}, \quad n = 1,2,...N_{\phi yy},$$
$$i = (m-1)N_{\phi yy} + n, \quad N_{\phi y} = N_{\phi yx} N_{\phi yy}$$

where the superscripts on $f(x)$ and $g(y)$ indicates the associated variable: w, ϕ_x, or ϕ_y.

Stiffener Representation

In the following paragraphs the boundary conditions for a simply supported loaded end is considered, the shape functions are identified, and the resulting expressions for the matrix elements (equations (32)) are listed. In those expressions, δ_{ij} is the Kronecker delta function, for which

$$\delta_{ij} = \begin{cases} 1 & i = j \\ 0 & i \neq j \end{cases} \tag{35}$$

and for a typical matrix element, we use the notation

$$K_{ij}^{k\ell} = K_{mnrs}^{k\ell} \tag{36}$$

implying that i is a function of m and n by the relations given in equations (39), and j is a function of r and s in the same manner.

The boundary conditions used for this case are

$$
\begin{aligned}
&w(0,y) = w(\ell, y) = w(x,0) = 0 \\
&\phi_x(x,0) = 0 \\
&\phi_y(0,y) = \phi_y(\ell, y) = 0
\end{aligned}
\tag{37}
$$

and assuming a nominal half-wave buckling mode shape, the additional conditions are specified to discount any contributions not symmetric in x about the line $x = L/2$:

$$
\begin{aligned}
&x\left(\frac{\ell}{2} + \Delta, y\right) = w\left(\frac{\ell}{2} - \Delta, y\right) \\
&\phi_x\left(\frac{\ell}{2} + \Delta, y\right) = -\phi_x\left(\frac{\ell}{2} - \Delta, y\right) \\
&\phi_y\left(\frac{\ell}{2} + \Delta, y\right) = \phi_y\left(\frac{\ell}{2} - \Delta, y\right)
\end{aligned}
\tag{38}
$$

The following shape functions are used:

$$
\begin{aligned}
\psi_i(x,y): &\quad f_m(x) = \sin(2m-1)\pi\frac{x}{\ell} \;\; ; \;\; g_n(x) = y^n \\
\theta_{xi}(x,y): &\quad f_m(x) = \cos(2m-1)\pi\frac{x}{\ell} \;\; ; \;\; g_n(x) = y^n \\
\theta_{yi}(x,y): &\quad f_m(x) = \sin(2m-1)\pi\frac{x}{\ell} \;\; ; \;\; g_n(x) = y^{(n-1)}
\end{aligned}
\tag{39}
$$

and when the integrals of equations (32) are evaluated, the following expressions result:

$$
K_{ij}^{11} = K_{mnrs}^{11} = K^2 A_{55} I_1 + K^2 A_{44} I_2 \tag{40 - a}
$$

where

$$
\begin{aligned}
I_1 &= (2m-1)^2 \frac{\pi^2}{2\ell} \frac{b^{(n+s+1)}}{(n+s+1)} \delta_{mr}, \\
I_2 &= \frac{\ell}{2} \frac{nsb^{(n+s-1)}}{(n+s-1)} \delta_{mr}
\end{aligned}
$$

$$K_{ij}^{12} = K_{mnrs}^{12} = K^2 A_{55}(2m-1)\frac{\pi}{2}\frac{b^{(n+s+1)}}{(n+s+1)}\delta_{mr}$$

$$K_{mnrs}^{13} = K^2 A_{44}\frac{\ell}{2}\frac{nb^{(n+s-1)}}{(n+s-1)}\delta_{mr} \qquad (40-b)$$

$$K_{mnrs}^{22} = D_{11}I_1 + D_{66}I_2 = K^2 A_{55}I_3$$

where

$$I_1 = [(2m-1)\pi]^2\frac{1}{2\ell}\frac{b^{(n+s+1)}}{(n+s+1)}\delta_{mr}$$

$$I_2 = \frac{\ell}{2}\frac{nsb^{(n+s-1)}}{(n+s-1)}\delta_{mr}$$

$$I_3 = \frac{\ell}{2}\frac{b^{(n+s+1)}}{(n+s+1)}\delta_{mr}$$

$$K_{mnrs}^{23} = D_{12}I_1 + D_{66}I_2 \qquad (40-c)$$

where

$$I_1 = -(2m-1)\frac{\pi}{2}\frac{(s-1)^{(n+s-1)}}{(n+s-1)}\delta_{mr}$$

$$I_2 = (2m-1)\frac{\pi}{2}\frac{nb^{(n+s-1)}}{(n+s-1)}\delta_{mr}$$

$$K_{mnrs}^{33} = D_{22}I_1 + D_{66}I_2 + K^2 A_{44}I_3 \qquad (40-d)$$

where

$$I_1 = \left\{\begin{array}{l} \dfrac{\ell}{2}\dfrac{(n-1)(s-1)h^{(n+s-3)}}{(n+s-3)}\delta_{mr}, \quad n>1, \quad s>1, \\ 0, \quad n=1 \text{ or } s=1 \end{array}\right\}$$

$$I_2 = [(2m-1)\pi]^2\frac{1}{2\ell}\frac{b^{(n+s-1)}}{(n+s-1)}\delta_{mr}$$

$$I_3 = \frac{\ell}{2}\frac{b^{(n+s-1)}}{(n+s-1)}\delta_{mr}$$

Summary of Buckling Considerations

The equations governing the buckling of a uniaxially loaded orthotropic stiffener were developed using a first order shear deformation theory for plates. An approximate solution procedure was developed and implemented on a computer using the Rayleigh-Ritz method, for plates with simply supported loaded ends. The method also adapts easily to the treatment of uniaxially loaded orthotropic plates with other boundary conditions. This method can be used in conjunction with a stability analysis of triangular sub-elements of the panel skin to form a local buckling criteria for designing grid stiffened plates. Currently, buckling analysis of panel skin sub-components between the stiffeners is under way.

FIGURE 1

GRID STIFFENED COMPOSITE PANEL
&
REPRESENTATIVE UNIT CELL

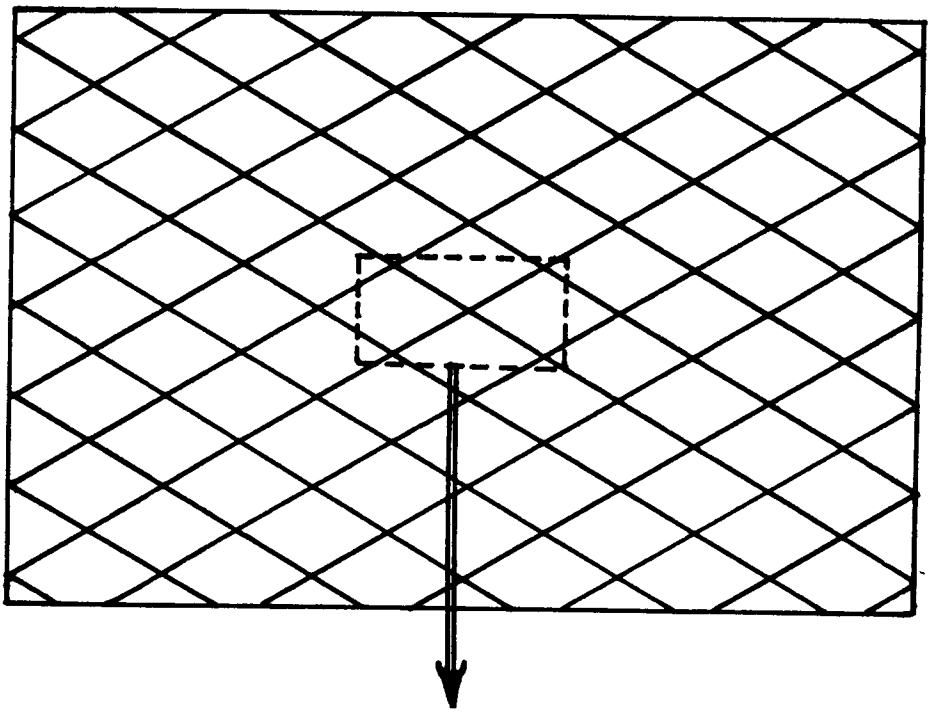

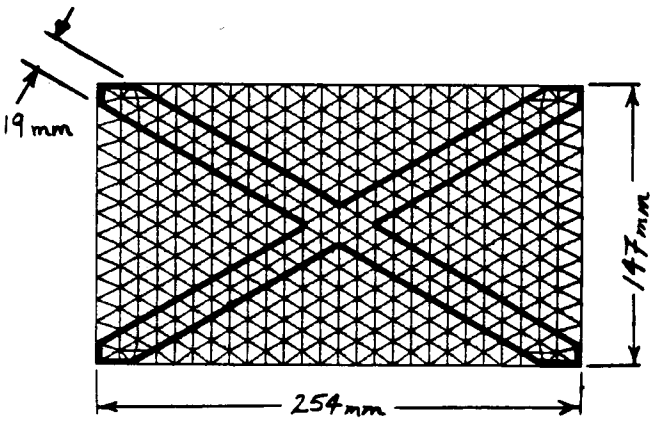

FIGURE 2

TRANSVERSE DISPLACEMENT OF FREE EDGES

60 DEGREE STIFFENED PANEL
LONGITUDINAL FREE EDGES
STIFFENER RATIO = 10
UNIT AXIAL DISPLACEMENT
DISPLACEMENTS X 50

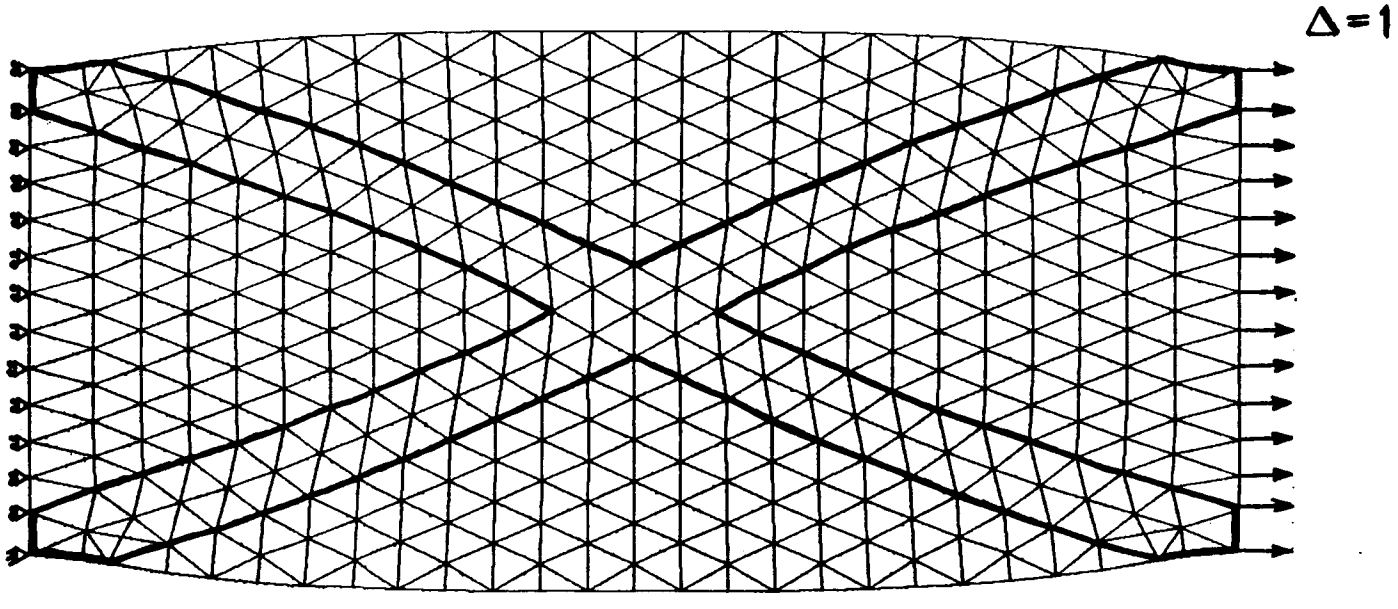

FIGURE 3

EFFECT OF LONGITUDINAL RESTRAINT BEAMS

60 DEGREE STIFFENED PANEL
LONGITUDINAL RESTRAINT BEAMS
STIFFENER RATIO = 10
UNIT AXIAL DISPLACEMENT
DISPLACEMENTS X 50

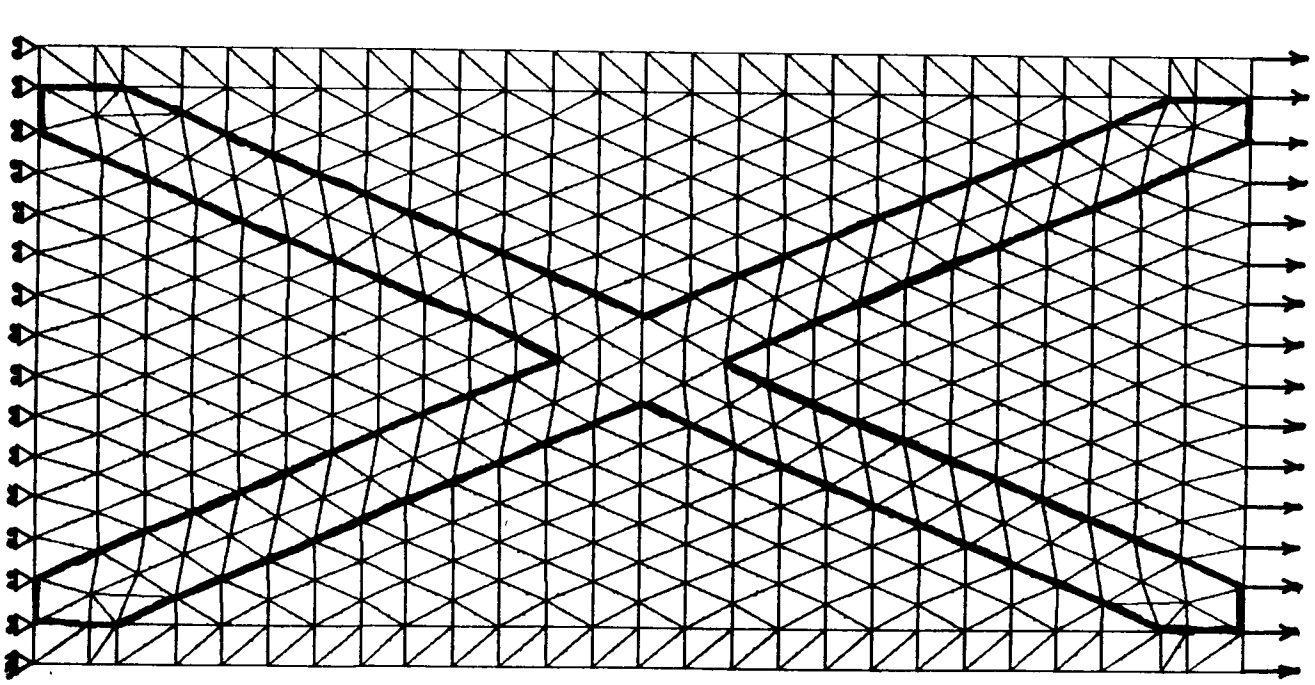

FIGURE 4

AXIAL STIFFNESS VS STIFFENER RATIO

WITH & WITHOUT EDGE RESTRAINT

60 DEGREE STIFFENED PANELS
UNIT AXIAL DISPLACEMENT

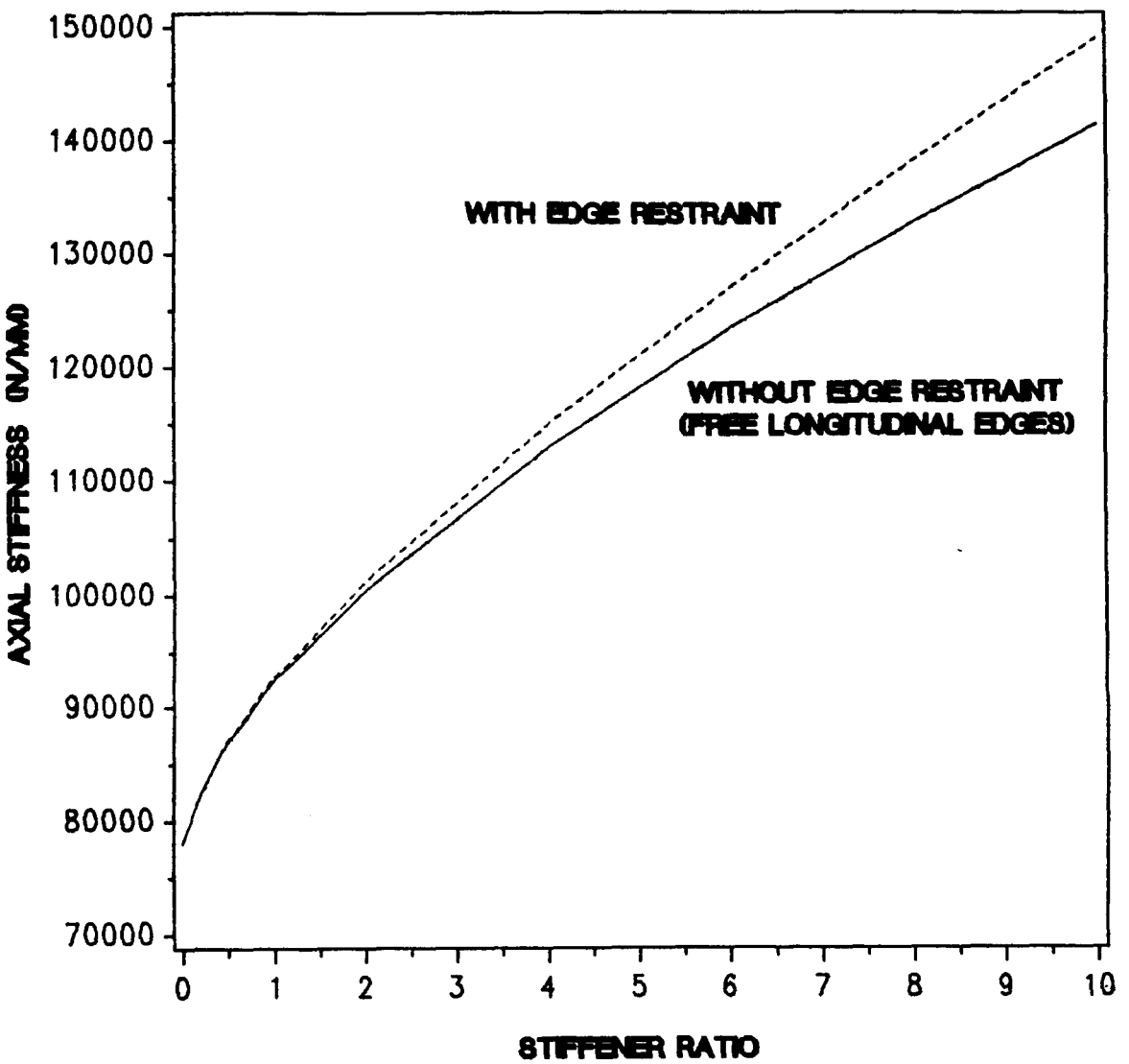

FIGURE 5

SPECIFIC AXIAL STIFFNESS VS STIFFENER RATIO

60 DEGREE STIFFENED PANELS
LONGITUDINAL RESTRAINT BEAMS
UNIT AXIAL DISPLACEMENT

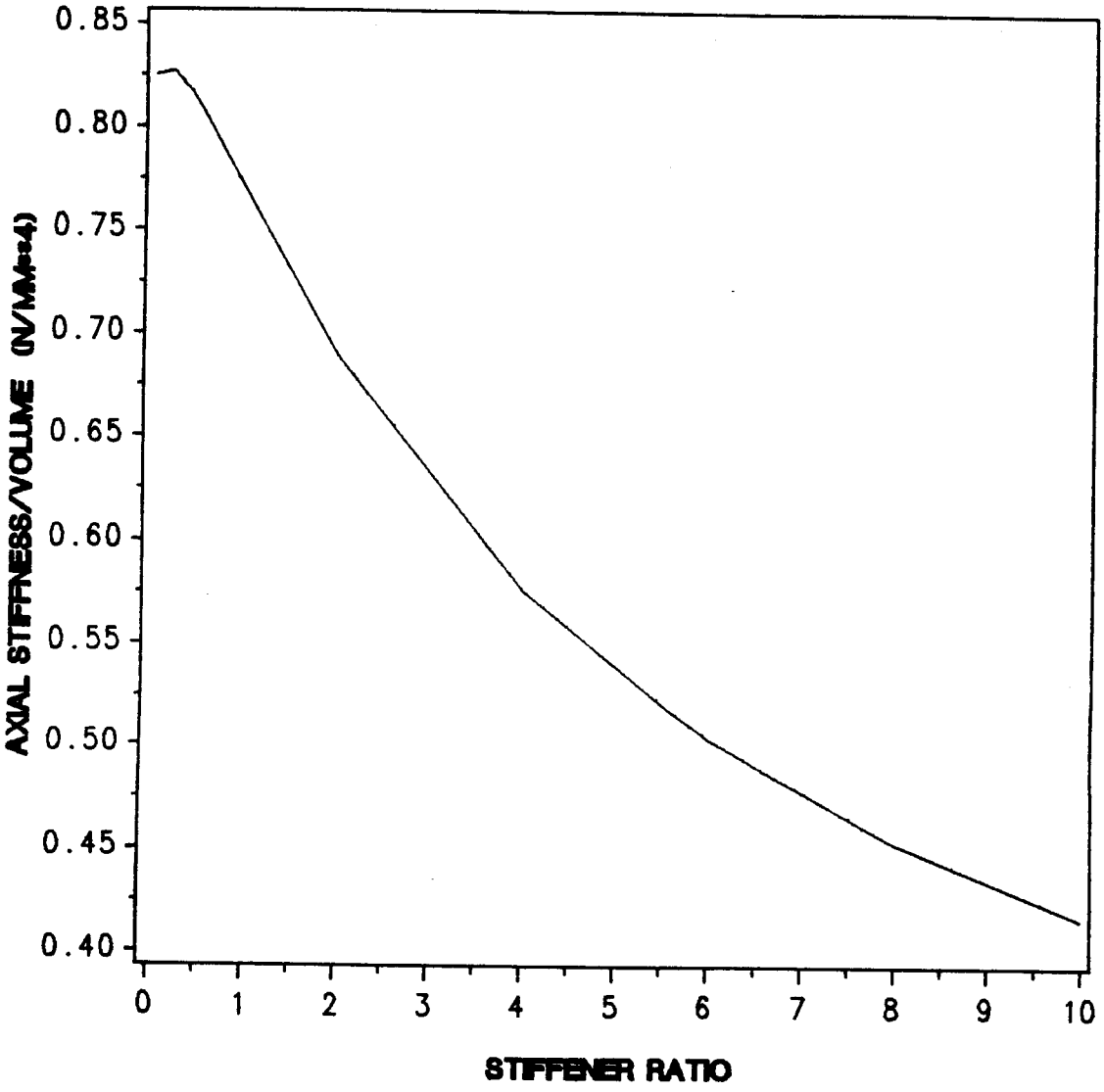

FIGURE 6

TRANSVERSE CONTRACTION OF LATTICE GRID

60 DEGREE LATTICE GRID
LONGITUDINAL RESTRAINT BEAMS
SKIN PROPERTIES = 0
UNIT AXIAL DISPLACEMENT
DISPLACEMENTS X 50

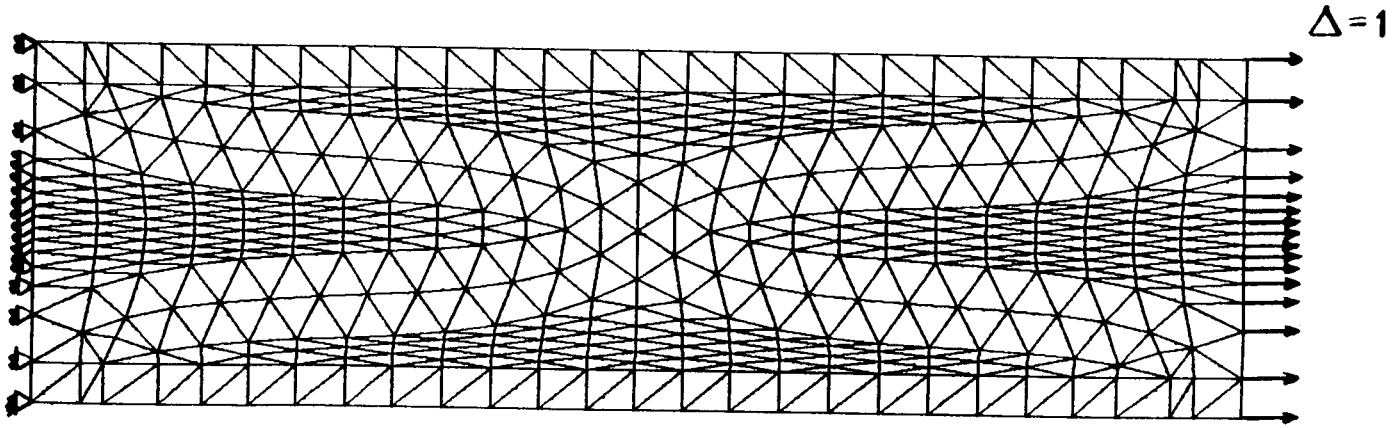

FIGURE 7

STIFFENER MODULI VS STIFFENER RATIO

(30/0/+45/-45/90)
GRAPHITE/EPOXY

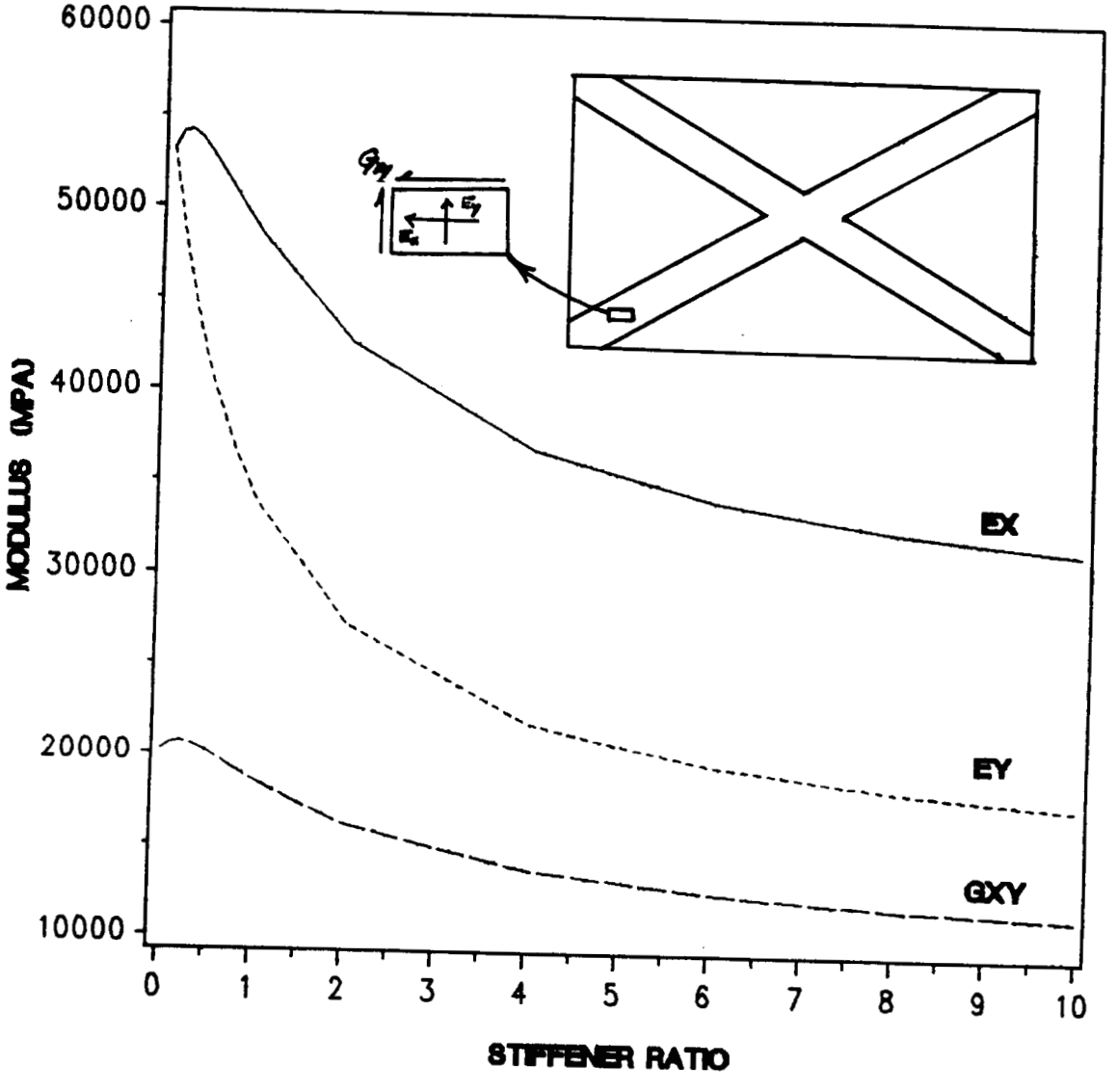

FIGURE 8

TYPICAL STIFFENED SHEAR PANEL

60 DEGREE STIFFENED PANEL
FOUR EDGE RESTRAINT BEAMS
STIFFENER RATIO = 10
UNIT DIAGONAL DISPLACEMENT
DISPLACEMENTS X 50

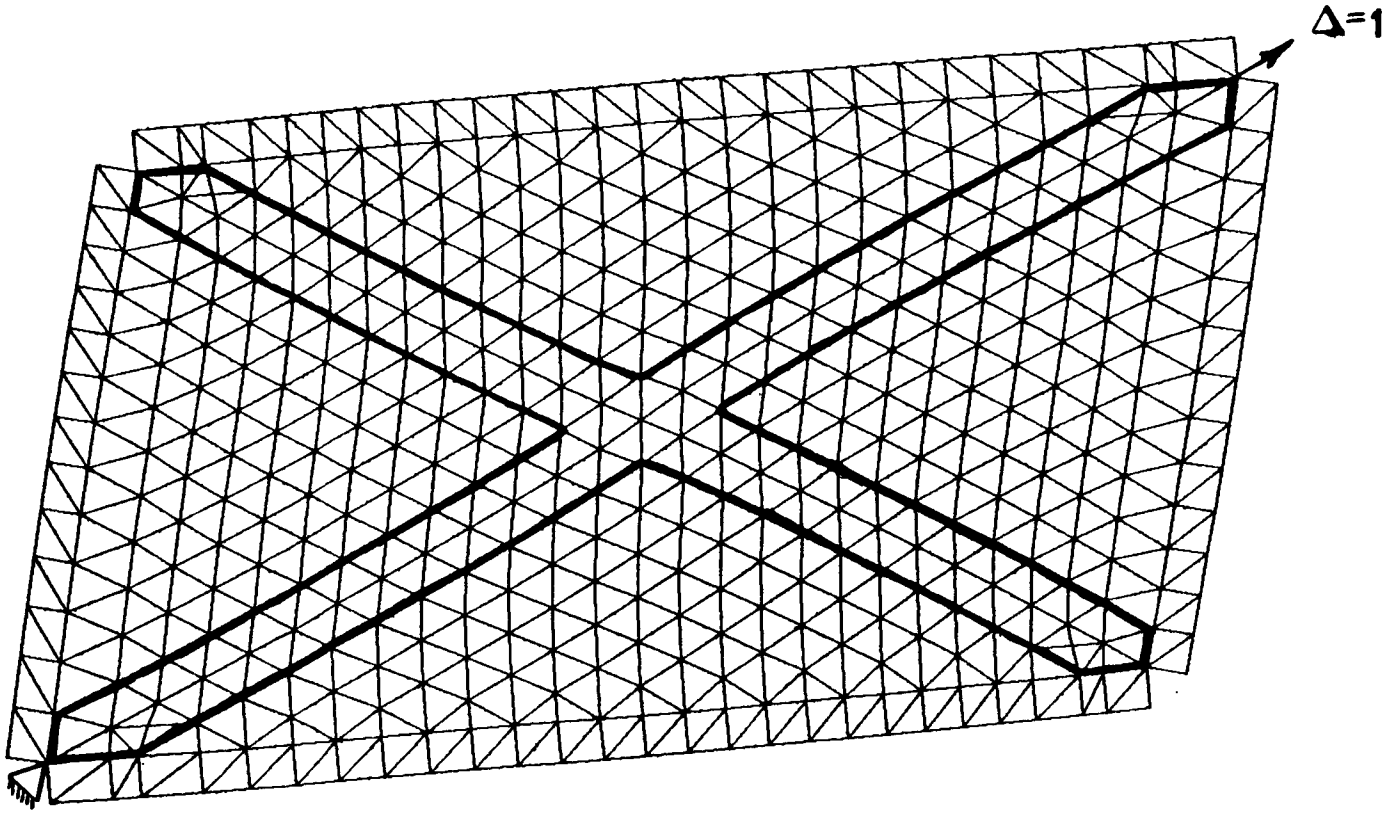

FIGURE 9

SHEAR STIFFNESS VS STIFFENER RATIO

60 DEGREE STIFFENED PANELS
FOUR EDGE RESTRAINT BEAMS
UNIT DIAGONAL DISPLACEMENT

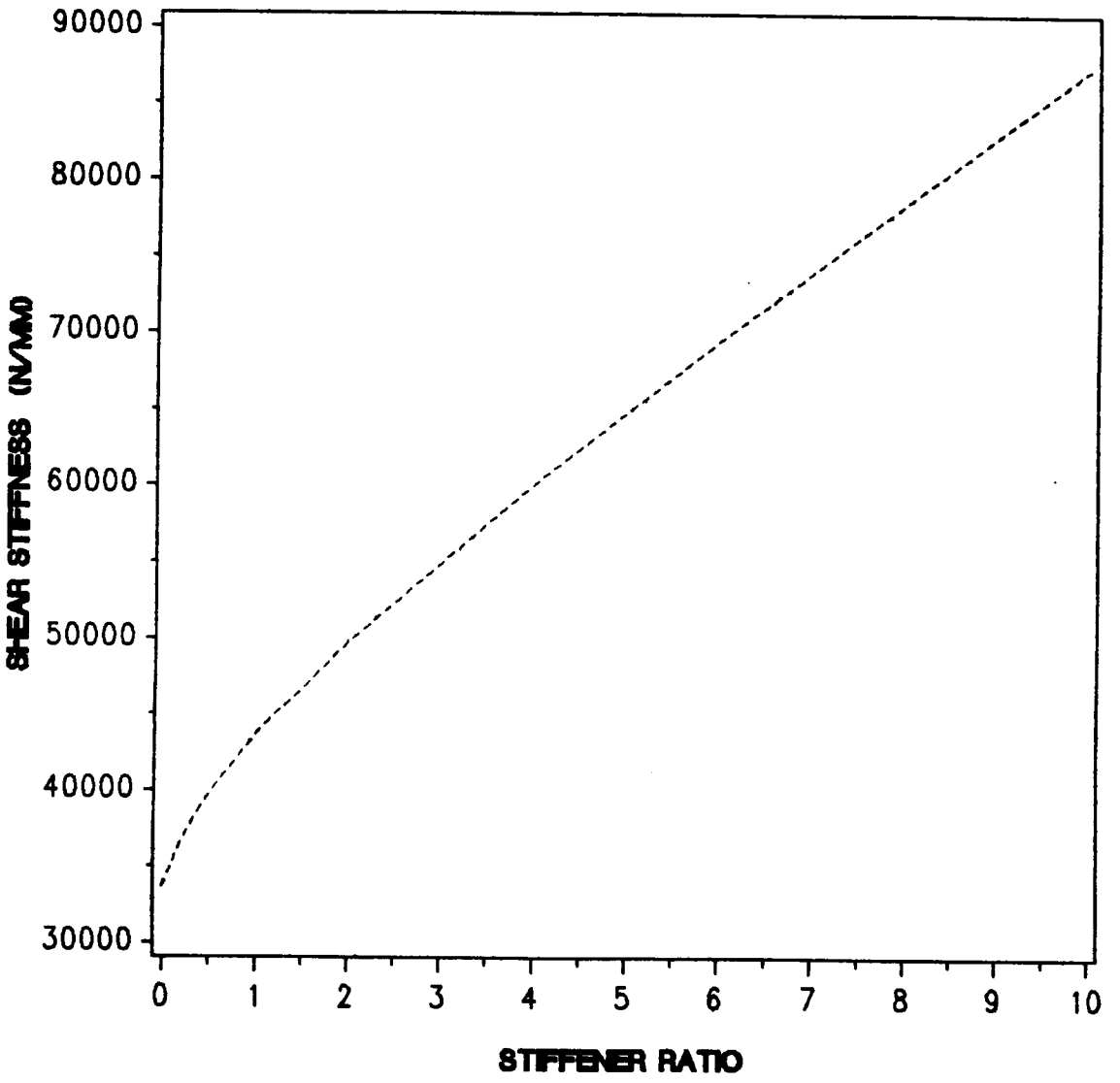

FIGURE 10

SPECIFIC SHEAR STIFFNESS VS STIFFENER RATIO

60 DEGREE STIFFENED PANELS
FOUR EDGE RESTRAINT BEAMS
UNIT DIAGONAL DISPLACEMENT

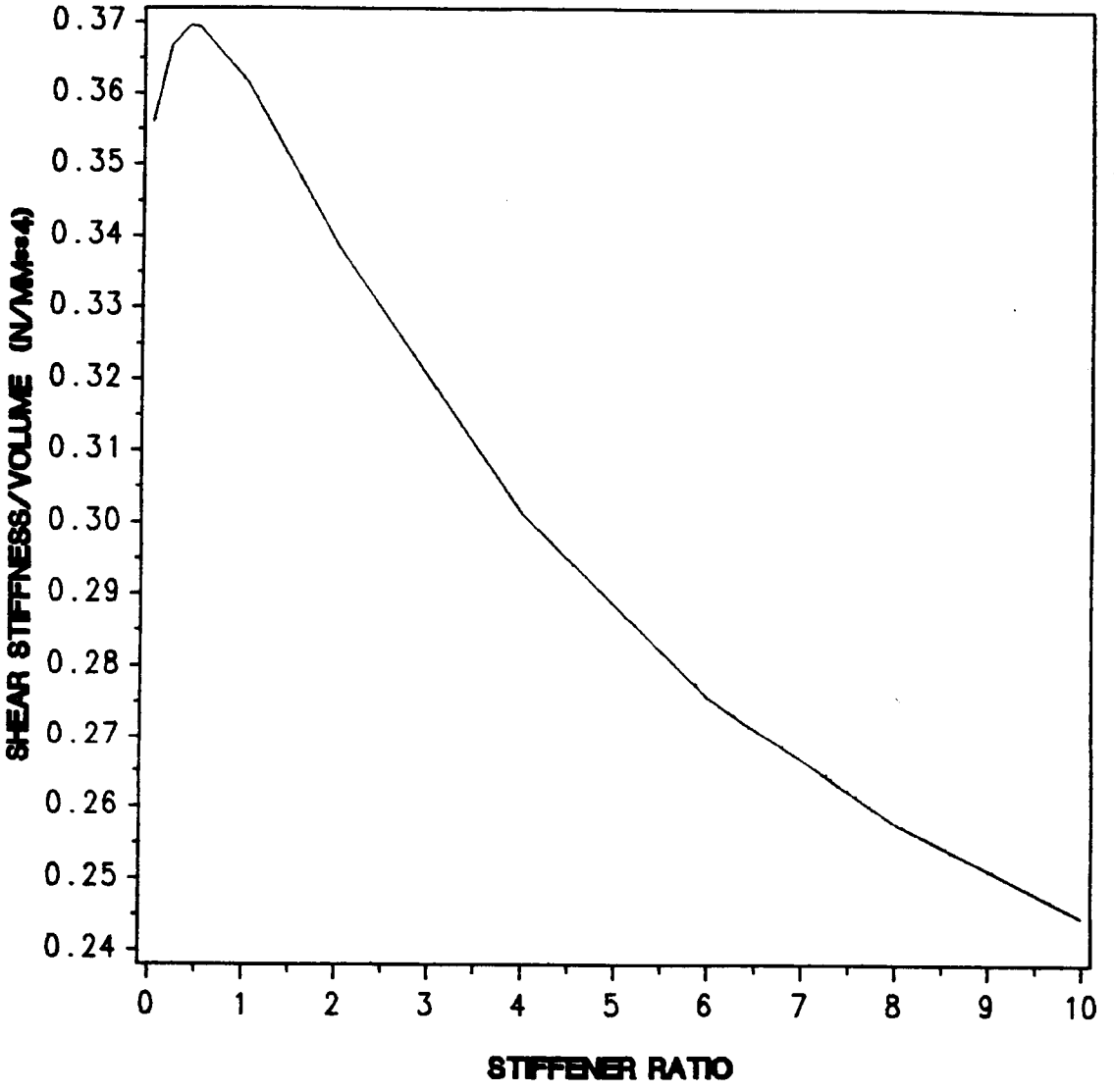

FIGURE 11

LATTICE GRID WITH SHEAR LOAD

60 DEGREE LATTICE GRID
FOUR EDGE RESTRAINT BEAMS
SKIN PROPERTIES = 0
UNIT DIAGONAL DISPLACEMENT
DISPLACEMENTS X 50

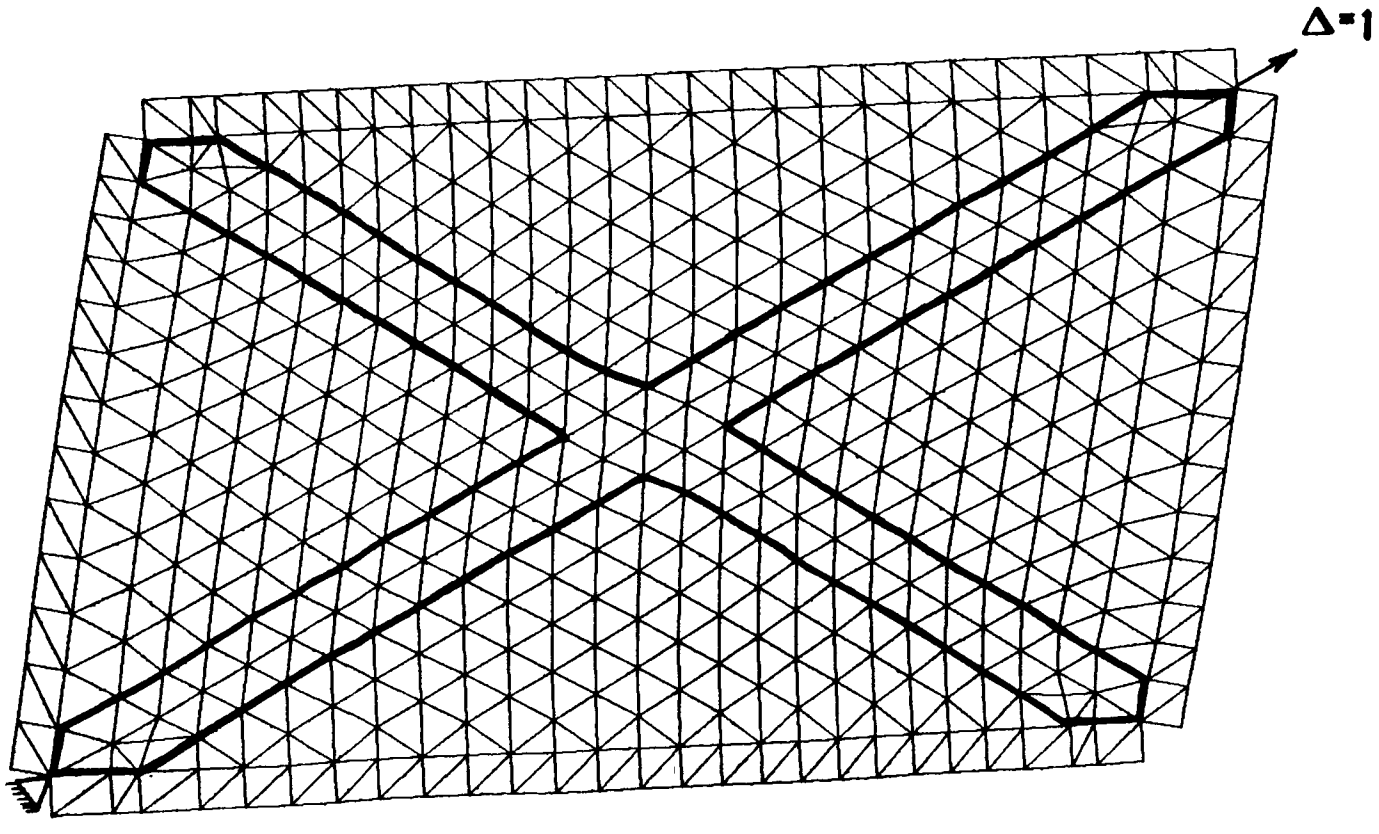

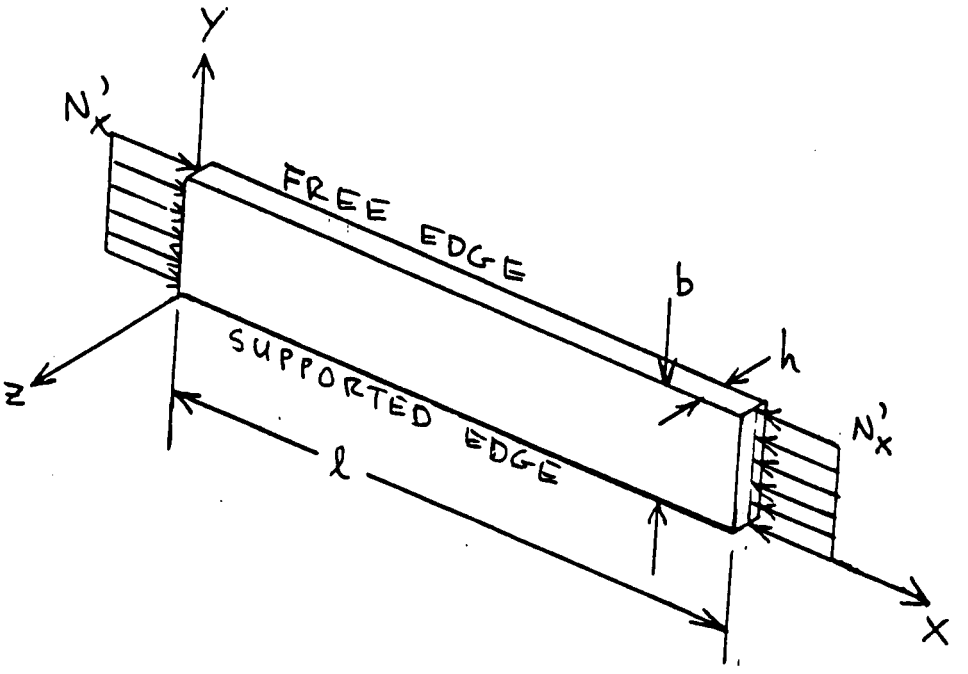

Fig. 12 : **Labeling conventions for end-loaded stiffener.**